Hindawi
Shock and Vibration
Volume 2024, Article ID 1948140, 13 pages
https://doi.org/10.1155/2024/1948140

Research Article

Calculation of Temperature Action of Flat Steel Box Girder of Long-Span Bridges Using a Joint Model of ARMA Mean and GARCH Variance

Jun Yang[1], **Dacheng Zhao**[1], **Bin Chen**[1] and **Gaoxin Wang**[2]

[1]*China Railway Bridge & Tunnel Technologies Co. Ltd, Nanjing 210032, China*
[2]*China University of Mining and Technology, Xuzhou 221116, China*

Correspondence should be addressed to Gaoxin Wang; civilgxwangg@hotmail.com

Received 9 November 2023; Revised 6 March 2024; Accepted 28 March 2024; Published 26 April 2024

Academic Editor: Chengwei Fei

Using the monitoring temperature field data from the flat steel box girder, the time histories of temperature data and temperature difference data are investigated using the extreme value analysis method. Because the calculation of standard values of temperature action needs massive temperature field data, the simulation of daily extreme values of temperature data and temperature difference data is carried out by virtual of Probability Statistical Method. The seasonal and nonstationary trend terms are described using the weighted sum of a series of basic elementary functions. The random fluctuation term is represented by a joint model of ARMA mean and GARCH variance. Moreover, the yearly extreme values of temperature data and temperature difference data are considered as statistical variables, and their standard values of temperature action with 50-year return period are calculated by means of the general extreme value (GEV) distributive function. The research results can supply references for temperature action of flat steel box girder.

1. Introduction

Because flat steel box girders are becoming more and more common in large-span bridge structures, it is important to study the standard values of temperature action for flat steel box girders [1–5]. However, current bridge researchers still have insufficient understanding of the standard values of temperature action in flat steel box girders [6–12]. The China bridge design codes also do not specify the calculation method of standard values of temperature action in flat steel box girders. To determine the standard value of temperature action, the bridge engineers often take the annual extreme values of measured temperature or temperature difference data as statistical variables, but the number of measured temperature data is usually not enough for statistical analysis [13–15]. How to use the measured temperature data to calculate the standard values of temperature action becomes one urgent problem. In addition, some latest monitoring results indicate that there is a nonnegligible transverse temperature difference in the top plate of flat steel box girder, but the China bridge specification code does not provide the standard value for this type of temperature difference [16–19]. Therefore, a clear understanding of standard values of temperature action for flat steel box girder of long-span bridges can provide an important reference for thermal design of flat steel box girders of long-span bridge structures.

In view of this, one suspension bridge is taken as research object. Based on the monitoring data from the flat steel box girder, the extreme value analysis is employed to investigate the time-varying characteristics of daily extreme values of temperatures and temperature differences. Then, the mathematical modeling method is used to simulate the daily extreme values of temperatures and temperature differences for 50 years, with description of seasonal trend term and nonstationary trend term in the daily extreme values as the ARMA and GARCH combined model. Furthermore, the annual extreme values of temperatures and temperature

differences are taken as statistical variables, and one distribution function called generalized extreme value is used to calculate the standard values of temperature action within 50-year return period.

2. Monitoring Results of Temperature Field in Steel Box Girder

2.1. Monitoring Section and Sensor Deployment. The bridge is a suspension bridge, and the main girder is a flat steel box girder, as shown in Figure 1. This bridge is located at Zhenjiang City, Jiangsu Province, crossing the Yangtze River, and this region belongs to a subtropical monsoon climate with distinct four seasons, abundant heat, and abundant rainfall. The design dimensions of girder section are 37.4 m in width, 3.0 m in height, 14 mm in thickness of top plate, and 12 mm in thickness of bottom plate. Using the health monitoring system installed on the bridge, the temperature data from flat steel box girder are measured. To be specific, eight measurement locations are shown in Figure 1, which are denoted by C1~C8, respectively. The sampling frequency of the temperature sensor is 1 Hz.

2.2. Monitoring Results. Taking the measuring point C1 as an example, its time history in the whole year 2022 is shown in Figure 2(a). It can be seen that it shows significant seasonal variation characteristics, and the highest temperature value can reach 48.0°C. Figure 2(b) further gives a period of time history of C1 on January 28, 2022, which presents significant daily variation characteristics similar to the shape of a single-period sine curve. Considering that the standard value of temperature action belongs to the category of extreme value analysis, the one-year variation of daily maximum and minimum values of C1 is further shown in Figures 3(a) and 3(b), respectively. It can be seen that the maximum and minimum values fluctuate randomly around the seasonal variation characteristics.

Taking C1 and C3 as an example, the temperature difference can be obtained after two temperature values of C1 and C3 at the same time are subtracted, as shown in Figure 4(a). It can be seen that the negative temperature difference reaches −10.4°C. Figure 4(b) further gives a period of temperature difference on April 6, 2022, which presents a daily variation characteristic similar to the shape of a single-period cosine curve. Furthermore, the one-year time histories of daily maximum and minimum temperature differences are shown in Figures 5(a) and 5(b), respectively. It can be seen that they present random variation characteristics, not like the changing trends of temperatures as shown in Figures 3(a) and 3(b).

3. Probability Statistical Properties of Temperature Differences

3.1. Probability Statistical Method. Based on the monitoring temperature data, the mathematical statistics method is used to analyze the cumulative probability of vertical and horizontal positive and negative temperature differences. The best cumulative distribution function is selected to fit the cumulative probability of temperature differences.

The change of temperature differences with time is regarded as a stationary stochastic process with the same distribution. The daily positive and negative extreme values of temperature differences are selected as random variables. The normal distribution (normal distribution), EV distribution (extreme value distribution), and GEV distribution (generalized extreme value distribution) are selected to fit the daily positive and negative extreme values of temperature differences.

In detail, the cumulative distribution function of normal distribution is calculated as follows:

$$f(x) = \frac{1}{\sqrt{2\pi}\sigma}\int_{-\infty}^{x} e^{-\left((x-\mu)^2/2\sigma^2\right)}\mathrm{d}x. \tag{1}$$

The cumulative distribution function of extreme value distribution is calculated as follows:

$$f(x) = \frac{1}{\lambda}e^{\left[-(x-k/\lambda)-e^{(-x-k/\lambda)}\right]}. \tag{2}$$

The cumulative distribution function of the generalized extreme value distribution is calculated as follows:

$$f(x) = e^{\left\{-[1+\mathrm{K}(x-\mu/\sigma)]^{(1/-k)}\right\}I(T)}, \tag{3}$$

wherein

$$\mathrm{I(T)} = \begin{cases} 1 & \left[1+\dfrac{K(x-\mu)}{\sigma}\right] > 0, \\ 0 & \left[1+\dfrac{K(x-\mu)}{\sigma}\right] \le 0. \end{cases} \tag{4}$$

In the formula, λ is the proportion coefficient, k is the shape parameter, σ is the scale parameter, μ is the position parameter, and λ, k, σ, and μ can be estimated using the least square method.

In order to compare the fitting effects of three distribution functions, the fitting errors $E_{\max}$ and $E_{\min}$ of three functions are calculated as follows:

$$E_{\max} = \frac{\sqrt{\sum_{j=1}^{n}\left[P_{\max}\left(T_{\max}(j)\right) - P_{\max}\left(T_{\max}(j)\right)\right]^2}}{n}, \tag{5}$$

$$E_{\min} = \frac{\sqrt{\sum_{j=1}^{n}\left[P_{\mathrm{m,r}}\left(T_{\mathrm{dmin}}(j)\right) - P_{\mathrm{m,s}}\left(T_{\mathrm{dmin}}(j)\right)\right]^2}}{n}. \tag{6}$$

In the formula, $P_{m,r}(T_{\mathrm{dmax}}(j))$ and $P_{m,s}(T_{\mathrm{dmax}}(j))$ are the measured and simulated cumulative probabilities of the positive temperature differences on the jth day, respectively; $P_{m,r}(T_{\mathrm{dmin}}(j))$ and $P_{m,s}(T_{\mathrm{dmin}}(j))$ are the measured and simulated cumulative probabilities of negative temperature differences on the jth day, respectively; and n represents the total number of temperature extreme value samples.

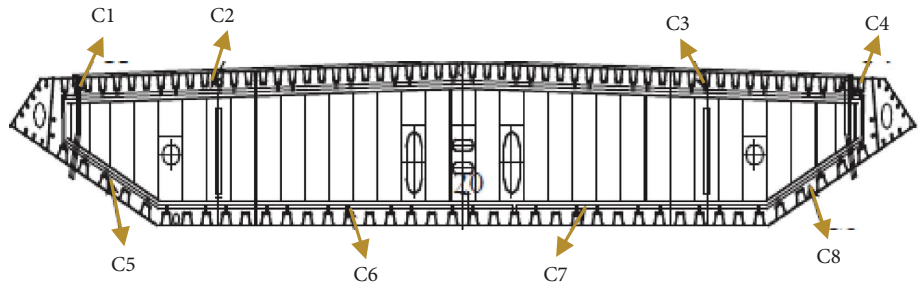

Figure 1: Deployment of temperature sensors in the flat steel box girder.

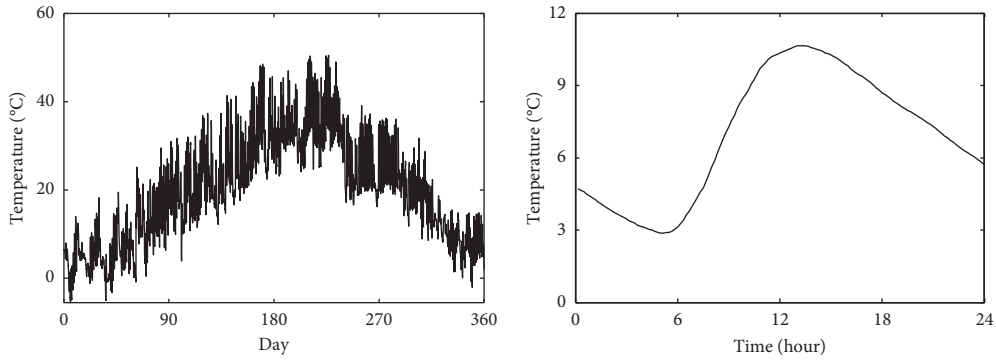

Figure 2: Time history of C1. (a) The time history in the whole year 2022. (b) The time history on January 28, 2022.

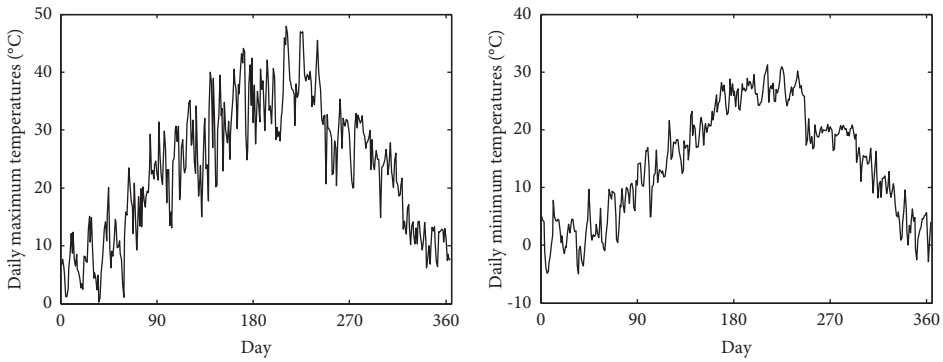

Figure 3: Time histories of daily maximum and minimum temperatures. (a) The one-year variation of daily maximum values. (b) The one-year variation of daily minimum values.

3.2. Probability Statistical Results. First, the cumulative probabilities of daily extreme values of temperature differences are fitted using normal, EV, and GEV distribution functions, respectively. The fitting results are shown in Figure 6. $T_{ij,p}$ denotes the daily positive extreme values of temperature differences between C_i and C_j, and $T_{ij,n}$ denotes the daily negative extreme values of temperature differences between C_i and C_j. Then, the fitting errors of the three distribution functions are calculated according to equations (5) and (6), and the calculation results are shown in Table 1.

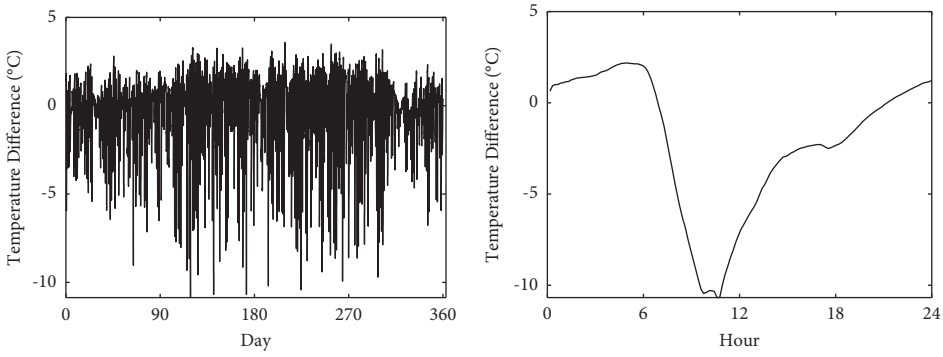

Figure 4: Time histories of temperature differences between point C1 and point C3. (a) The time history in the whole year 2022. (b) The time history on January 28, 2022.

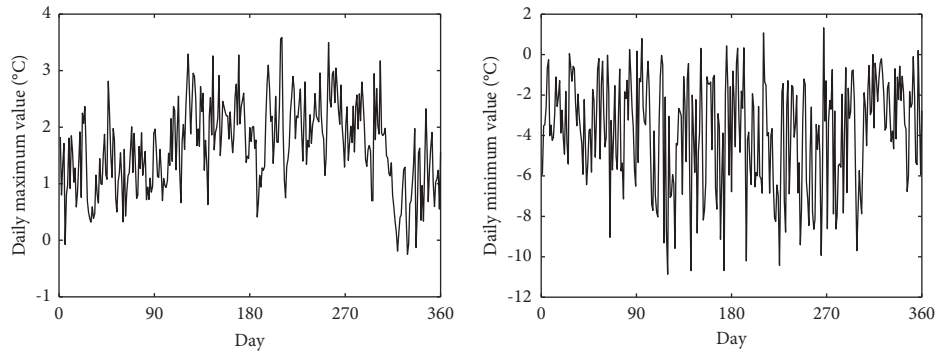

Figure 5: Time histories of daily maximum and minimum temperature differences. (a) The one-year variation of daily maximum values. (b) The one-year variation of daily minimum values.

By comparing the fitting error values of three cumulative distribution functions on temperature samples, it can be found that the fitting error of the GEV distribution function is smaller than the other fitting errors. Therefore, the GEV distribution is selected as the cumulative distribution function of the statistical variable.

4. Modeling Method for Time Series of Temperature Field

4.1. Modeling Theory. When calculating the standard values of temperature action, the annual extreme values of temperatures and temperature differences are commonly used as statistical variables. However, the measured data can only provide the annual extreme values of temperatures and temperature differences in the year 2022, so the annual extreme values for many years should be simulated to guarantee enough number of annual extreme values for probabilistic statistical analysis. The annual extreme values are taken from the time histories of daily extreme values, which contain seasonal and random variation characteristics. These variation characteristics can be simulated using a mathematical model regarding time series analysis.

The seasonal variation characteristics can be mathematically described by a weighted sum of a series of elementary functions (such as sine function, cosine function, exponent function, and power function) as follows:

$$A(t) = \sum_{N=0}^{n} M_i H(t, N). \tag{7}$$

In this formula, $A(t)$ denotes the daily extreme values in the tth day regarding seasonal variation characteristics; $H(t, N)$ denotes an elementary function; M_i denotes a weighting coefficient; and n denotes the order.

The random variation characteristics contain autoregressive characteristics, moving average characteristics, and heteroscedasticity characteristics. These three characteristics can be described by a mean-variance model, where the mean portion of model can reflect the autoregressive characteristics and moving average characteristics, which is expressed as follows [20]:

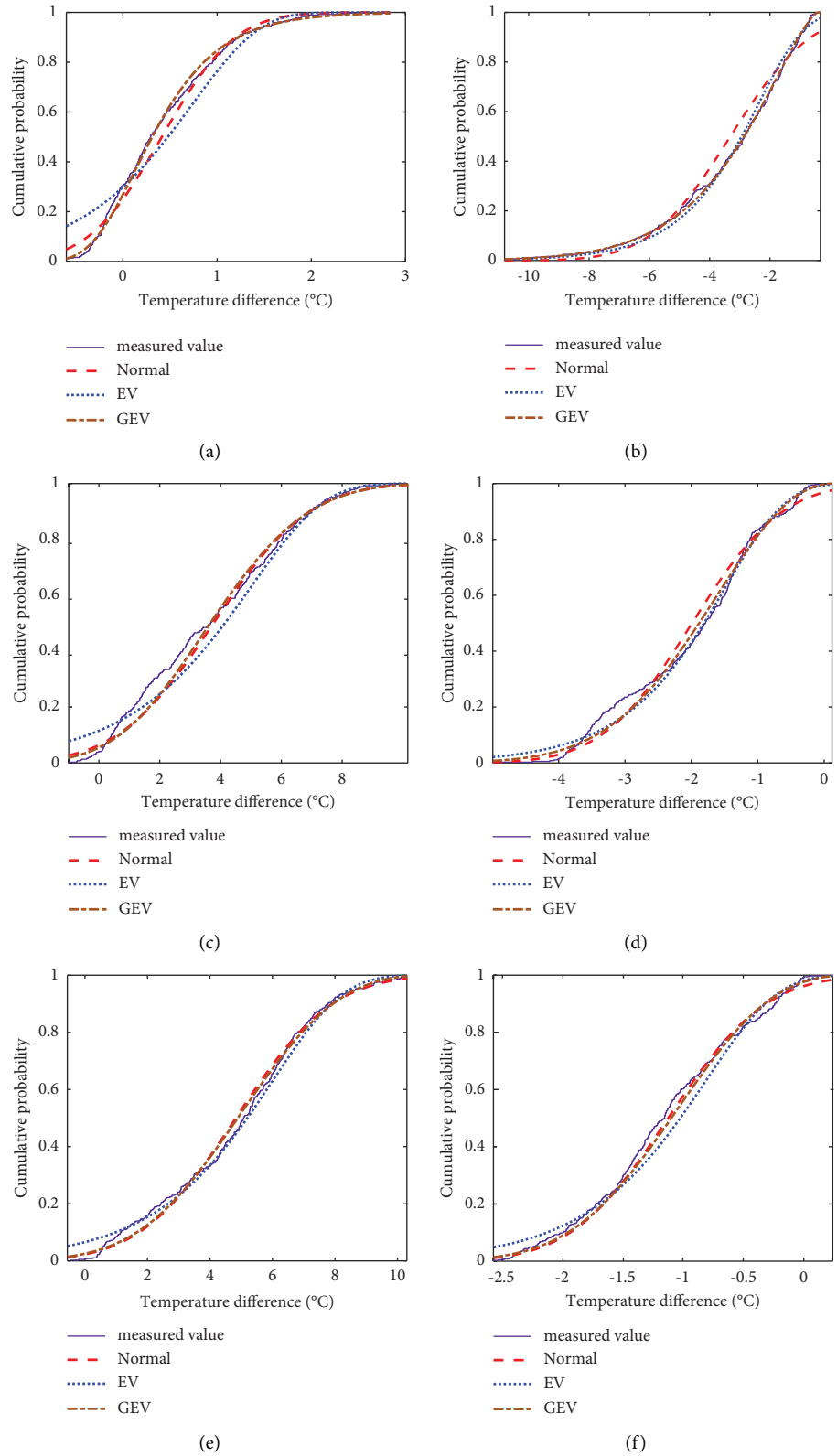

Figure 6: Continued.

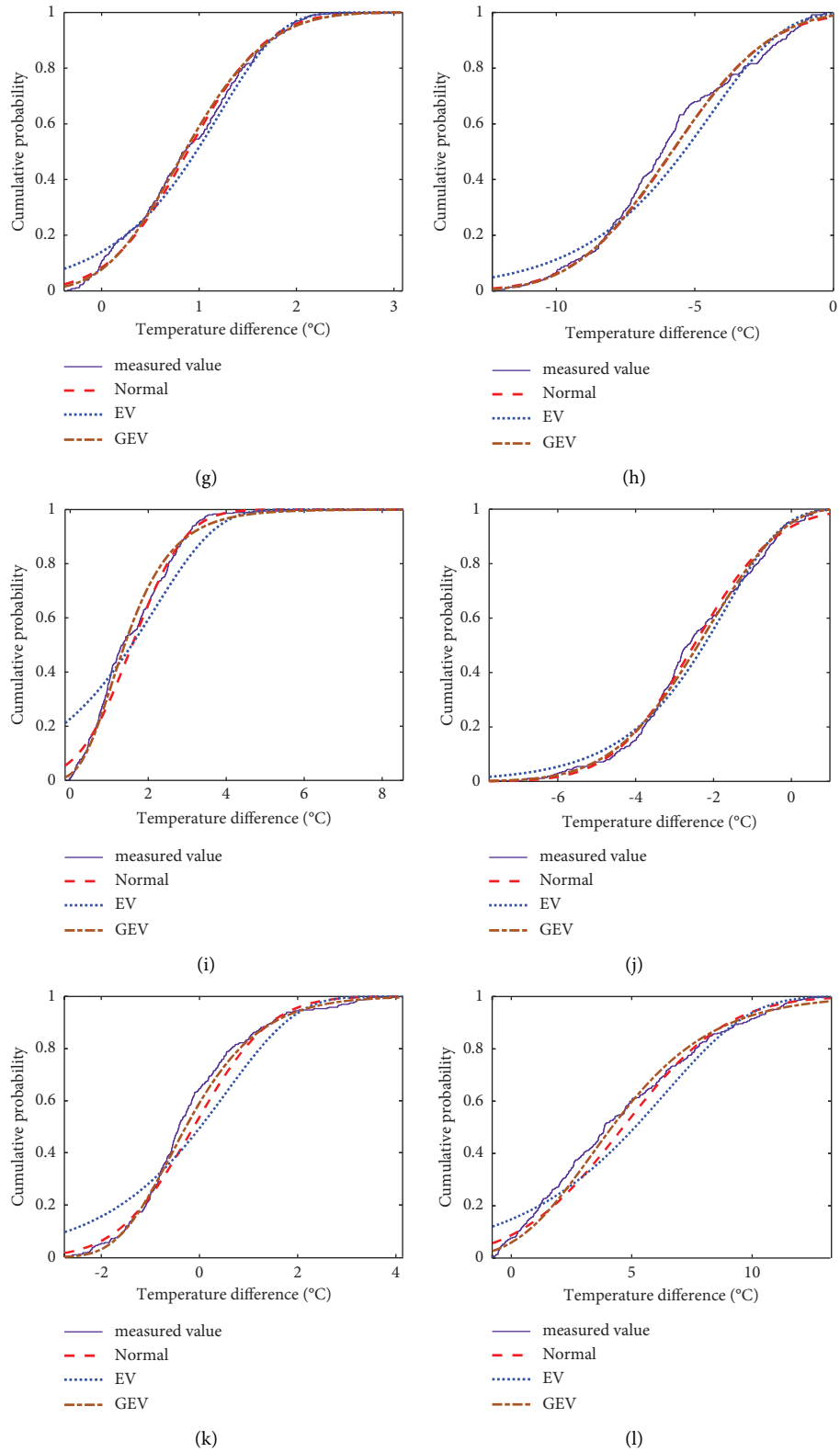

Figure 6: The cumulative probabilities of daily extreme values. (a) $T_{12,p}$, (b) $T_{12,n}$, (c) $T_{13,p}$, (d) $T_{13,n}$, (e) $T_{23,p}$, (f) $T_{23,n}$, (g) $T_{34,p}$, (h) $T_{34,n}$, (i) $T_{35,p}$, (j) $T_{35,n}$, (k) $T_{37,n}$, (l) $T_{37,p}$.

Table 1: Fitted errors of three cumulative distribution functions.

Fitted errors	Temperature differences	Normal	EV	GEV
$E_{\max}$	$T_{12,p}$	0.0023	0.0040	0.0011
	$T_{13,p}$	0.0019	0.0023	0.0019
	$T_{23,p}$	0.0097	0.0013	0.0012
	$T_{34,p}$	0.0013	0.0019	0.0012
	$T_{35,p}$	0.0023	0.0052	0.0019
	$T_{37,p}$	0.0021	0.0033	0.0015
$E_{\min}$	$T_{12,n}$	0.0010	0.0019	0.0008
	$T_{13,n}$	0.010	0.0041	0.0032
	$T_{23,n}$	0.0022	0.0058	0.0011
	$T_{34,n}$	0.0016	0.0064	0.0014
	$T_{35,n}$	0.0228	0.0033	0.0013
	$T_{37,n}$	0.0070	0.0023	0.0013

$$A_t = c + \sum_{j=1}^{p} b_j H_{t-j} + \sum_{j=0}^{q} c_j \varepsilon_{t-j}. \quad (8)$$

In the formula, A_t denotes the daily extreme values in the tth day regarding random variation characteristics; c denotes the constant term; p and q denote the autoregressive order and the moving average order, respectively; b_j and c_j denote the autoregressive coefficient and moving average coefficient, and the value of c_0 is 1; and ε_{t-j} denotes the white noise with a time delay of j. Equation (8) is simply referred to as ARMA (p, q) model [20].

The variance portion of model can reflect the heteroscedasticity characteristics, which is expressed as follows:

$$\sigma_t^2 = \kappa + \sum_{k=1}^{m} g_k \sigma_{t-k}^2 + \sum_{k=1}^{n} \nu_k \varepsilon_{t-k}^2, \quad (9)$$

with the restrictions: $\sum_{k=1}^{p} g_k + \sum_{k=1}^{n} \nu_k < 1$; $\kappa > 0$; $g_k > 0$; $\nu_k > 0$.

In the formula, σ_t denotes the variance values in the tth day regarding random variation characteristics; k denotes the constant term; m and n denote the autoregressive order and the moving average order of the variance model, respectively; and g_k and ν_k denote the autoregressive and moving average coefficients, respectively. Equation (9) is simply referred to as the GRACH (m, n) model [20]. ARMA (p, q) model combined with GRACH (m, n) is called the mean-variance model.

4.2. Modeling Steps. Because the daily extreme values of temperatures and temperature differences have the same modeling steps, the temperature data from C6 are selected for illustration of modeling steps.

4.2.1. Modeling of Seasonal Variation Characteristics. The one-year time history of the daily minimum values from C6 is shown in Figure 7. The least square fitting is utilized to fit the seasonal variation characteristics based on equation (7), and some elementary functions, i.e., the first-order Fourier series, the first-order Gauss series, and the second-order power exponential polynomial, are used for curve fitting as shown in Figure 7. It can be seen that the Fourier series fit the best, which can be used to describe the seasonal variation characteristics, and the estimated parameter values of Fourier series are shown in Table 2.

4.2.2. Modeling of Random Variation Characteristics. Time series of the random variation characteristics is obtained by measured temperatures minus fitted temperatures using equation (7), as shown in Figure 8. The method of establishing the mean-variance model for random variation characteristics is illustrated in the following steps:

Step 1: Stationary Characteristic Test. A good stationary characteristic is the precondition for establishing the mean-variance model. For this reason, the autocorrelation function ρ and the partial correlation function β within 30-step time lag are calculated as shown in Figures 9(a) and 9(b), respectively. It can be seen that both of them decay rapidly to 95% confidence interval, which shows that the random variation characteristics have good stationary characteristics. In addition, the unit root of time history data is calculated using the augmented Dickey–Fuller test, and the results reject the null hypothesis of a unit root against the autoregressive alternative, which indicates that the random variation characteristics have good stationary characteristics.

Step 2: Order Determination of Mean-Variance Model. The orders p and q of the mean model in equation (8) are related to the decay form of autocorrelation function ρ and partial correlation function β. It can be seen from Figure 8 that the autocorrelation function ρ shows obvious trailing property, while the partial correlation function β shows obvious two-step truncation property, so the mean model shown in equation (8) follows ARMA (2, 0) model [20]. Furthermore, the Engle test is carried out for the heteroscedasticity of the random variation characteristics, and the results rejected null hypothesis of no conditional heteroscedasticity, which concluded that there are significant heteroscedasticity effects in the random variation characteristics. Then, the order of variance model shown in equation (9) is further determined using AIC and BIC criteria. To be specific, the statistical values of

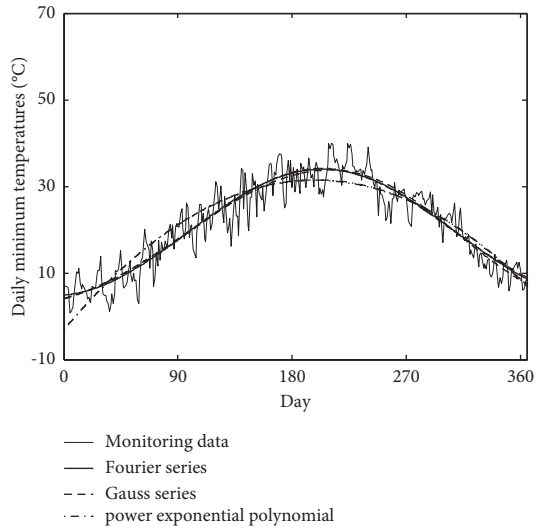

Figure 7: Seasonal variation trend and its fitting curve.

Table 2: Values of estimated parameters in Fourier series.

Fourier series	$A(t) = a_0 + a_1\cos(wt) + a_2\sin(wt)\ (0 \le t \le 365)$			
Parameters	a_0	a_1	a_2	w
Values	14.610	−12.35	−3.258	0.016

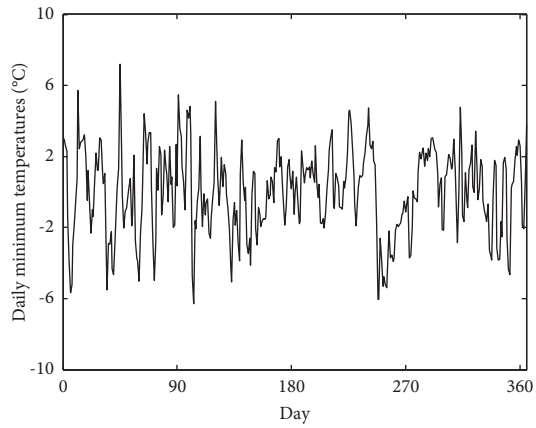

Figure 8: Time series of the random variation characteristics.

AIC and BIC within the first five order values of m and n are calculated as shown in Figure 10. The orders of m and n corresponding to the minimum statistics values of AIC are selected from Figure 10(a): $m = 2$, $n = 1$, and the orders of m and n corresponding to the minimum statistics values of BIC are selected from Figure 10(b): $m = 1$, $n = 1$. Therefore, there are two combinations for the mean-variance model: (1) the combination of ARMA (2, 0) model and GARCH (2, 1) model; (2) the combination of ARMA (2, 0) model and GARCH (1, 1) model.

Step 3: Parameter Estimation for Mean-Variance Model. The estimated parameters are the autoregressive coefficient, the moving average coefficient, and the constant term in equations (8) and (9), which can be calculated using the maximum likelihood estimation method. Finally, the mean-variance model for description of random variation characteristics is determined using the estimated parameter values.

4.2.3. Model Verification. Based on the modeling analysis above, the one-year time history of daily minimum temperature values from C6 is mathematically simulated by two types of combinations. The first type of combination is the first-order Fourier series, ARMA (2, 0) and GARCH (2, 1); the second type of combination is the first-order Fourier series, ARMA (2, 0) and GARCH (1, 1). In order to verify the simulation effect, the residuals between simulated and

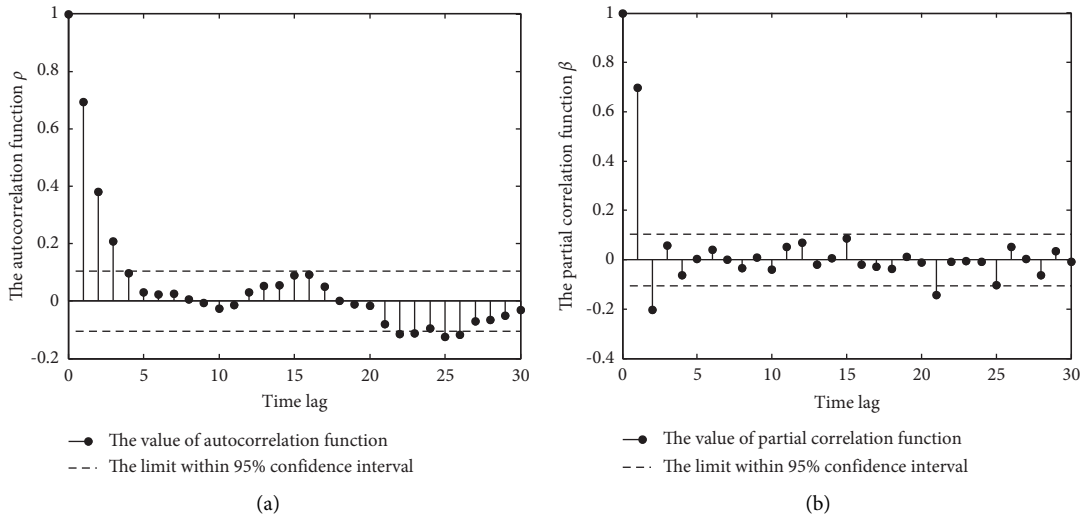

Figure 9: Autocorrelation function and partial correlation function within 30-step time lag. (a) The autocorrelation function ρ. (b) The partial correlation function β.

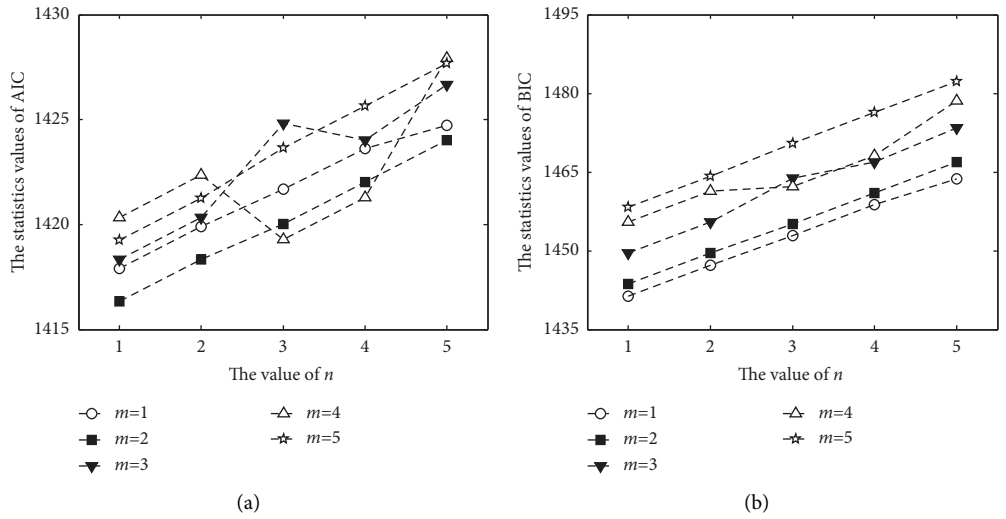

Figure 10: The statistics values of AIC and BIC within the first five order values. (a) The statistics values of AIC. (b) The statistics values of BIC.

measured values are tested using autocorrelation function and partial correlation function, with the results shown in Figures 11 and 12, respectively. It can be seen that all the values of autocorrelation function and partial correlation function fall within the 95% confidence interval, indicating good simulation effect.

Furthermore, the 50-year time history of daily minimum temperature values is simulated using the mathematical model, and then the annual minimum temperature values in 50 years are selected, as shown in Figure 13, which can provide enough data for calculation of standard values of temperature action. What should be mentioned is that the time histories of temperature differences have stationary random characteristics, which are not affected by years, so one year of data is feasible to simulate annual extreme values if their stationary random characteristics are accurately grasped.

5. The Calculation Method of Temperature Standard Value

By referring to the European bridge design code, the standard value of temperature action refers to the characteristic value within a return period of 50 years. What should be mentioned is that "50 years" means the return period of temperature standard values not the design service life of

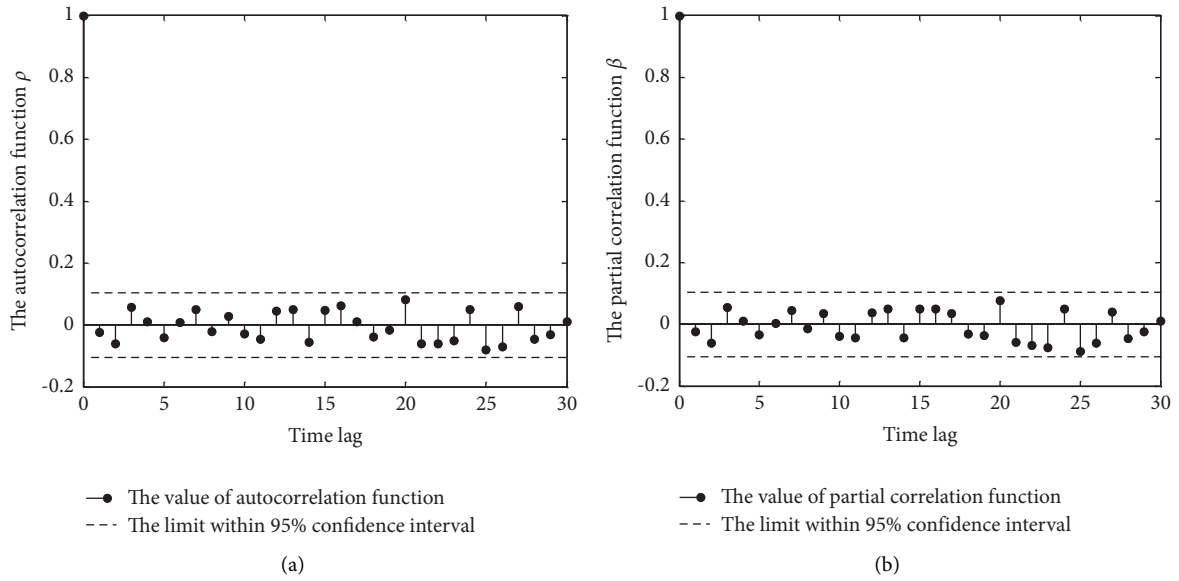

Figure 11: Autocorrelation function and partial correlation function for the first type of combination. (a) Autocorrelation function. (b) Partial correlation function.

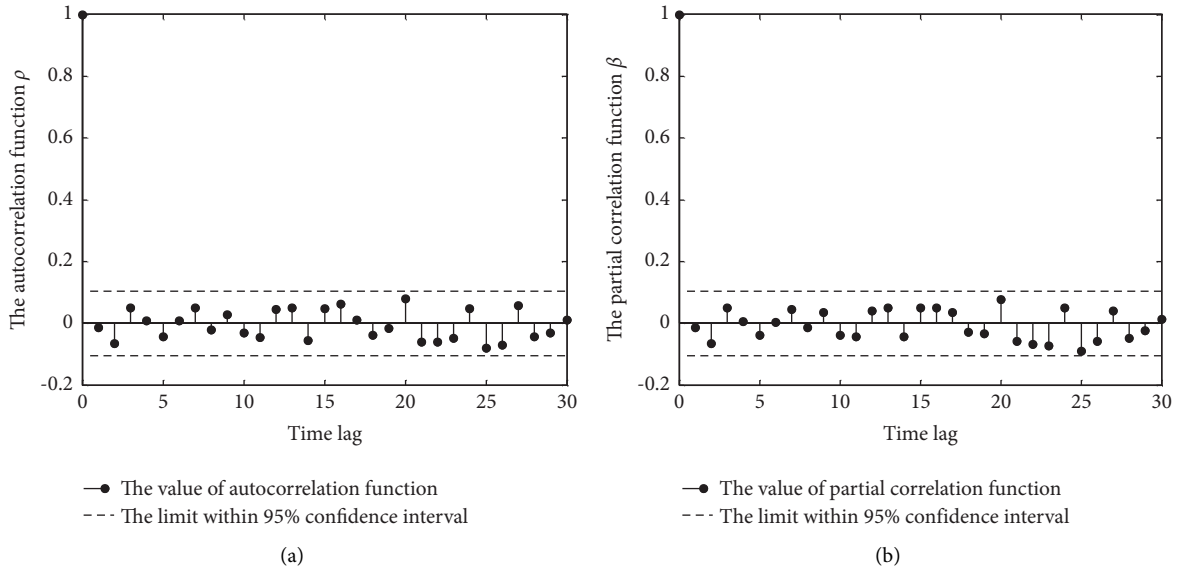

Figure 12: Autocorrelation function and partial correlation function for the second type of combination. (a) Autocorrelation function. (b) Partial correlation function.

long-span bridges. In addition, the standard value of the temperature action is commonly calculated using the statistical variable of yearly extreme values of temperatures or temperature differences, so the proceeding probability in the 50-year return period is 2%. The calculation formula for the standard value A_0 is shown as follows [21]:

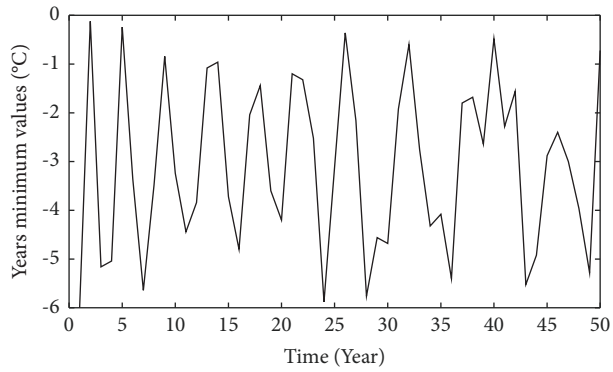

Figure 13: Time history of the annual minimum temperature values in 50 years.

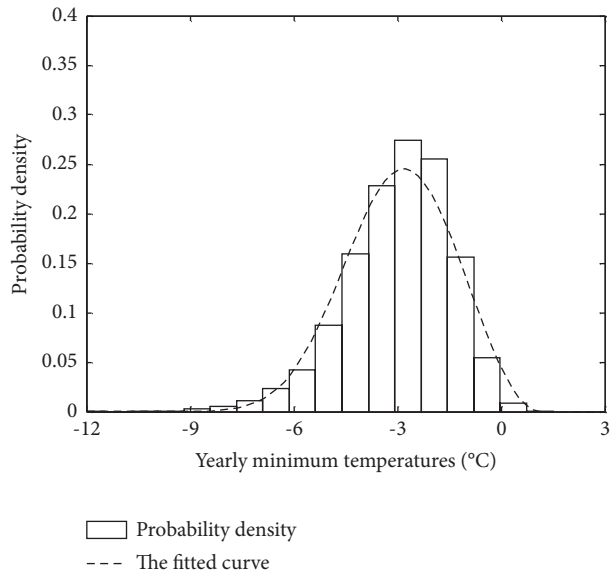

Figure 14: The probability density histogram and its fitted curve.

Table 3: The standard values of temperature differences.

Variables	Transverse temperature difference					Vertical temperature difference
	T_{12}	T_{13}	T_{23}	T_{34}	T_{35}	T_{37}
Maximum values (°C)	13.2	10.5	7.5	15.1	14.3	21.1
Minimum values (°C)	−9.9	−13.9	−15.5	−7.4	−4.2	−9.0

Table 4: The standard values of temperatures.

Variables	Temperatures in the bottom plates		
	T_6	T_7	T_8
Maximum values (°C)	53.7	54.1	53.4
Minimum values (°C)	−7.7	−7.5	−8.3

$$W = \int_{A_0}^{+\infty} F(A)dA \text{ for maximum standard values,} \quad (10a)$$

$$W = \int_{-\infty}^{A} F(A)dA \text{ for maximum standard values,} \quad (10b)$$

where W denotes the proceeding probability of 2%; T denotes the statistical variable of yearly extreme values of temperatures or temperature differences; and $F(A)$ denotes the probability density function of generalized extreme value distribution [22], with its expression as follows:

$$F(A) = \frac{1}{a}\left[1 + r\left(\frac{A-b}{a}\right)\right]^{-(1/r)-1} \exp\left[-\left[1 + r\left(\frac{A-b}{a}\right)\right]^{-(1/r)}\right], \quad (11)$$

where r, b, and a denote shape parameters, position parameters, and scale parameters, respectively. The parameter value can be determined using least square fitting. The standard value A_0 is calculated using the Newton iteration method, or a more convenient solution method is feasible to calculate A_0 by directly using MATLAB probability and statistics toolbox. What should be mentioned is that, because standard values are the most unfavorable values which are used for bridge safety evaluation and the maximum or minimum temperature values are more unfavorable than mean temperature values, the maximum temperature values or minimum temperature values are used for calculation of standard values.

Taking C6 as an example, the probability density of annual minimum temperature values in 50 years is shown in Figure 14, and then it is fitted by probability density function through least square fitting. The fitted probability density curve is shown in Figure 14, and it can be seen that the fitted curve is in good agreement with the probability density histogram. The estimated parameters are $r = -0.3534$, $b = -3.4630$, and $a = 1.6101$. Furthermore, the standard value of annual minimum temperature values is −6.3°C after calculation using the probability density function.

The standard values of the vertical temperature differences between top and bottom plates as well as the transverse temperature differences in the top plate are shown Table 3. Because significant temperature differences exist in the top steel plate as well as between top and bottom plates, Table 3 only shows the standard values of temperature differences. It can be seen that the transverse temperature differences contain obvious maximum and minimum standard values, which should be considered in the thermal action design. In addition, the maximum vertical standard values are significantly bigger than the maximum transverse standard values.

The standard values of temperatures in the bottom plate are shown in Table 4. Because significant uniform temperatures exist in the bottom plate, Table 4 only shows the standard values of temperatures. In the tables, A_{ij} denotes the standard value of temperature difference between two measuring points C_i and C_j, and A_k denotes the standard value of temperature from the measuring point C_k, $i, j = 1, 2, ..., 5$, $k = 6, 7, 8$.

According to the "Eurocode 1: Actions on structures" [23], it only specifies the maximum and minimum standard values of vertical temperature differences, which are 24°C and −6°C, respectively. This design code does not specify the transverse temperature differences. Therefore, the research results can help provide reference for thermal action design of flat steel box girder, especially the transverse temperature differences in the top plate.

6. Conclusion

Using the monitoring temperature data from the flat steel box girder of a suspension bridge, this research proposed one calculation method of standard values of temperature action for flat steel box girder of long-span bridges based on simulation of monitoring data. The main conclusions are as follows:

(1) The time history of temperature data presents significant seasonal variation characteristics, and the time history of temperature difference data presents significant random variation characteristics.

(2) The seasonal variation characteristics can be described by a weighted sum of a series of basic elementary functions, and the random variation characteristics can be described by combination of ARMA and GARCH models.

(3) The generalized extreme value distribution function can well fit the probability density histogram. The proposed modeling method can generate enough data for calculation of standard values of temperature action.

(4) This research provides the standard values of the vertical temperature differences between top and bottom plates, the transverse temperature differences in the top plate, and the standard values of temperatures in the bottom plate, which provide reference for thermal action design of flat steel box girder.

What should be mentioned is that the standard values calculated in this research are a case study from a steel box girder in the specific bridge site environment, and the standard values of steel box girders in different bridge site environment may be different, but the calculation method can still provide important reference for steel box girders in other bridge site environments.

Data Availability

The data used to support the findings of this study are available from the corresponding author upon request.

Conflicts of Interest

The authors declare that there are no conflicts of interest regarding the publication of this paper.

Acknowledgments

The authors gratefully acknowledge the National Natural Science Foundation of China (51908545).

References

[1] Xu Huang, J. Zhu, and Y. Li, "Temperature analysis of steel box girder considering actual wind field," *Engineering Structures*, vol. 246, Article ID 113020, 2021.

[2] Y. Deng, H. Ju, G. Zhong, A. Li, and Y. Ding, "A general data quality evaluation framework for dynamic response monitoring of long-span bridges," *Mechanical Systems and Signal Processing*, vol. 200, Article ID 110514, 2023.

[3] Q. Zhu, H. Wang, and B. F. Spencer, "Investigation on the mapping for temperature-induced responses of a long-span steel truss arch bridge," *Structure and Infrastructure Engineering*, vol. 20, no. 2, pp. 232–249, 2022.

[4] H. Li, Z. Zhang, and N. Deng, "Temperature field and gradient effect of a steel-concrete composite box girder bridge," *Advances in Materials Science and Engineering*, vol. 2021, Article ID 9901801, 16 pages, 2021.

[5] T. Tao, H. Wang, Q. Zhu, Z. Zou, J. Li, and L. Wang, "Long-term temperature field of steel-box girder of a long-span bridge: measurement and simulation," *Engineering Structures*, vol. 236, Article ID 111924, 2021.

[6] F. Zhang, J. Shen, and J. Liu, "Effect of encased concrete on section temperature gradient of corrugated steel web box girder," *Advances in Structural Engineering*, vol. 24, no. 11, pp. 2321–2335, 2021.

[7] Q. Zhu, H. Wang, B. F. Spencer, and J. Mao, "Mapping of temperature-induced response increments for monitoring long-span steel truss arch bridges based on machine learning," *Journal of Structural Engineering*, vol. 148, no. 5, Article ID 04022034, 2022.

[8] F. Guo, S. Zhang, and S. Duan, "Analysis of measured temperature field of unpaved steel box girder," *Applied Sciences*, vol. 12, no. 17, p. 8417, 2022.

[9] C. Wang, P. Zhang, G. Wu, and P. Li, "Thermal fatigue load models for fatigue design of steel box girder bridges," *Journal of Constructional Steel Research*, vol. 198, Article ID 107560, 2022.

[10] J. Song, K. Hu, X. F. Shi, and C. A. Yin, "Research on temperature load model of a modular cable-stayed bridge," *Bridge Maintenance, Safety, Management, Life-Cycle Sustainability And Innovations*, vol. 25, pp. 575–581, 2021.

[11] Z.-wei Wang, W.-ming Zhang, Yu-feng Zhang, and Z. Liu, "Temperature prediction of flat steel box girders of long-span bridges utilizing in situ environmental parameters and machine learning," *Journal of Bridge Engineering*, vol. 27, no. 3, 2022.

[12] Qi-A. Wang, C. B. Wang, and Z.-G. Ma, "Bayesian dynamic linear model framework for SHM data forecasting and missing data imputation during typhoon events," *Structural Health Monitoring-An International Journal*, vol. 41, 2022.

[13] W. D. Ma, B. Wu, D. Qin, B. Zhao, and X. Yang, "Statistical analyses of the non-uniform longitudinal temperature distribution in steel box girder bridge," *Buildings*, vol. 13, no. 5, p. 1316, 2023.

[14] Y. Deng, A. Q. Li, S. R. Chen, and D. M. Feng, "Serviceability assessment for long-span suspension bridge based on deflection measurements," *Structural Control and Health Monitoring*, vol. 25, no. 11, p. e2254, 2018.

[15] S. J. Huang, C. Z. Cai, X. He, and C. Li, "Comparison of the corrugated steel web composite box-girder and traditional girders regarding temperature field under solar radiation," *Engineering Structures*, vol. 291, Article ID 116419, 2023.

[16] Y. Deng, A. Q. Li, Y. Liu, and S. R. Chen, "Investigation of temperature actions on flat steel box girders of long-span bridges with temperature monitoring data," *Advances in Structural Engineering*, vol. 21, no. 14, pp. 2099–2113, 2018.

[17] D. Zheng, Z. D. Qian, D. X. Liu, X. F. Zhang, and Y. Liu, "Thermal field characteristics of reinforced concrete box girder during high-temperature asphalt pavement paving," *Transportation Research Record*, vol. 2672, no. 41, pp. 56–64, 2018.

[18] C. Q. Miao and C. H. Shi, "Temperature gradient and its effect on flat steel box girder of long-span suspension bridge," *Science China Technological Sciences*, vol. 56, no. 8, pp. 1929–1939, 2013.

[19] Y. L. Ding and A. Q. Li, "Temperature-induced variations of measured modal frequencies of steel box girder for a long-span suspension bridge," *International Journal Of Steel Structures*, vol. 11, no. 2, pp. 145–155, 2011.

[20] Q. Liu, G. L. Zhang, S. Ali et al., "SPI-based drought simulation and prediction using ARMA-GARCH model," *Applied Mathematics and Computation*, vol. 355, pp. 96–107, 2019.

[21] G. X. Wang and Y. L. Ding, "Research on monitoring temperature difference from cross sections of steel truss arch girder of Dashengguan Yangtze Bridge," *International Journal Of Steel Structures*, vol. 15, no. 3, pp. 647–660, 2022.

[22] G. D. Zhou, T. H. Yi, B. Chen, and H. Zhang, "A generalized Pareto distribution-based extreme value model of thermal gradients in a long-span bridge combining parameter updating," *Advances in Structural Engineering*, vol. 20, no. 2, pp. 202–213, 2017.

[23] En, *Eurocode 1: Actions on Structures-Part 1-5: General Actions-Thermal Actions*, European Committee of Standardization, Brussels, Belgium, 2003.